

Quantum imaging by coherent enhancement

Guang Hao Low, Theodore J. Yoder, and Isaac L. Chuang

*Center for Ultracold Atoms, Research Laboratory of Electronics, and Department of Physics,
Massachusetts Institute of Technology, Cambridge, Massachusetts 02139, USA*

(Dated: September 30, 2014)

Conventional wisdom dictates that to image the position of fluorescent atoms or molecules, one should stimulate as much emission and collect as many photons as possible. That is, in this classical case, it has always been assumed that the coherence time of the system should be made short, and that the statistical scaling $\sim 1/\sqrt{t}$ defines the resolution limit for imaging time t . However, here we show in contrast that given the same resources, a long coherence time permits a higher resolution image. In this quantum regime, we give a procedure for determining the position of a single two-level system, and demonstrate that the standard errors of our position estimates scale at the Heisenberg limit as $\sim 1/t$, a quadratic, and notably optimal, improvement over the classical case.

The precise imaging of the location of one or more point objects is a problem ubiquitous in science and technology. While the resolution of an image is typically defined through the diffraction limit as the wavelength $\sim \lambda$ of illuminating light, the final estimate of object position instead exhibits a shot-noise limited precision σ that scales with the number of scattered photons detected – a consequence of the law of large numbers. Thus, in the absence of environmental noise, it is the time allowed for accumulating statistics that appears to limit the precision of position measurements.

Surprisingly, when the objects to be imaged are imbued with quantum properties, these well-known classical limits on resolution and precision can be improved. Impressive sub-optical resolutions of $\sim \frac{\lambda}{10}$ [1, 2] are obtainable by advanced microscopy [2] protocols such as STED [3], RESOLFT [4], STORM [5], and PALM [6]. Each in its own way exploits the coherence of a quantum object by storing its position x_i in its quantum state $|\psi\rangle$ over an extended period of time. Ultimately however, even for state-of-art, it is still the statistical scaling $\sigma \sim \frac{1}{\sqrt{t}}$ that limits the precision of a position estimate taking time t .

Yet, fundamentally, coherent quantum objects allow for a precision scaling quadratically better, as $\sigma \sim \frac{1}{t}$. This so-called Heisenberg limit [7] is a fundamental restriction of nature that bounds the precision of a single-shot phase estimate of $|\psi\rangle$, i.e. given a single copy of $|\psi\rangle$, to $\sim \frac{1}{t}$, a bound attainable in the regime of long coherence [8–10].

How then can quantum coherence be fully exploited to minimize the time required to obtain an estimate of a quantum object's position x_i with standard error σ ? An apparent contradiction arises since photon scattering rates approach zero in the limit of infinite coherence, in contrast to traditional imaging, where maximizing scattering is desirable. A similar problem arises in magnetic resonance imaging, but is there resolved by a two-step process: map x_i coherently to $|\psi\rangle$, and then read out $|\psi\rangle$ using just a few photons. However, current approaches have two flaws. First, the mapping is typically ambiguous (Fig. 1a). Due to the periodicity of quantum phases, multiple x_i can be encoded into the same observable of $|\psi\rangle$ – often the transition probability $s(x_i)$. Second, the

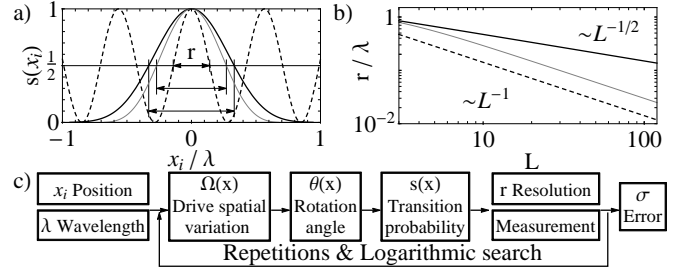


FIG. 1: a) Map from position x_i to transition probability $s(x_i)$. This is ideally unambiguous with a single narrow peak of width r (solid). The ambiguous map has multiple peaks (dashed). b) Scaling of r with the number of coherent drive pulses L . The optimal scaling is $\sim 1/L$ (dashed, thin), but often suboptimal $\sim 1/\sqrt{L}$ for unambiguous maps (thick). c) Procedure outline for estimating x_i with error σ scaling at the Heisenberg limit. This combines an optimal r -scaling unambiguous map with measurement in a logarithmic search.

mapping resolution r – the length scale over which $s(x_i)$ varies – cannot be improved arbitrarily in an effective manner. Doing so, with say a long sequence of L coherent excitations, either introduces more ambiguity or requires time that does not perform better than the statistical scaling (Fig. 1b). Approaches that estimate position with Heisenberg-limited scaling must overcome these two challenges.

Such well-known difficulties are apparent when using a spatially varying coherent drive, e.g. a gaussian beam, that produces excitations varying over space $\sim \lambda$. Due to projection noise [11], $s(x_i)$ can only be estimated with error scaling $\sim \frac{1}{\sqrt{t}}$. Thus for any given r , a precision $\sigma \sim \frac{r}{\sqrt{t}}$ results. Working around projection noise and improving these resolutions is the focus of much work in magnetic resonance as well quantum information science with trapped ions [12–17]. Unfortunately, state-of-art [13, 18, 19] excitation sequences, or pulse sequences, that produce a single unambiguous peak are sub-optimal – they offer a resolution of $r \sim \frac{\lambda}{\sqrt{L}}$ (Fig. 1) which is no better than the statistical scaling.

We present a new procedure that images quantum ob-

jects with precision $\sigma \sim \frac{1}{t}$, using a two-step imaging process which unambiguously maps spatial position to quantum state, allowing for readout with imaging resolution that scales as the optimum achievable by the Heisenberg limit. Like prior art, a pulse sequence is employed to implement the unambiguous mapping. In contrast though, we develop new sequences with the optimum resolution scaling $r \sim \frac{1}{L}$ (Fig. 1). Due to the narrowness of r , measuring the quantum state is much more likely to tell one where the object is not, rather than where it is located. Thus, our optimal unambiguous mapping alone is insufficient for achieving $\sigma \sim \frac{1}{t}$. However, this issue is neatly resolved using a logarithmic search, modeled after quantum phase estimation [8–10], that applies our mapping several times with varying widths. This logical flow (Fig. 1c) leads to our final result: an imaging algorithm with optimal precision $\sigma \sim \frac{1}{t}$. From the classical perspective that imaging should be done with short coherence times and maximal photon scattering, our algorithm is a complete surprise. In fact, our results imply that the best method for imaging quantum objects is to collect very few photons from a source that can be coherently controlled.

We begin by defining the resources required for imaging the position of a quantum object in one dimension. The action of pulse sequences on this system is briefly reviewed to demonstrate the mapping of spatial position to transition probability. This framework allows us to define the unambiguity and optimality criteria for a transition probability. We show that our new pulse sequences have both properties. These same properties also enable an efficient logarithmic search for system position, solving the projection noise issue. We then discuss estimates of real-world performance, generalizations to higher dimensions and multiple objects.

Consider a quantum two-level system with state $|\psi\rangle \in \text{SU}(2)$ at an unknown position $x_i \in I$ contained in a known interval I . Measurements in the $\{|0\rangle, |1\rangle\}$ basis are assumed, for simplicity. Provided is a coherent drive, over which we have phase ϕ and duration t control, with a known spatially varying Rabi frequency $\Omega(x)$, where $x = x_i - x_c$ can be translated by arbitrary distance x_c . With this coherent drive, a unitary rotation $U_\phi[\theta] = e^{-i\frac{\theta}{2}[\cos(\phi)\hat{X} + \sin(\phi)\hat{Y}]}$, where \hat{X}, \hat{Y} are Pauli matrices, that traverses angle $\theta(x) = \Omega(x)\tau$ can be applied to $|\psi\rangle$. Chaining L such discrete rotations generates a pulse sequence $\mathcal{S} = U_{\phi_L}[\theta] \dots U_{\phi_1}[\theta] \equiv (\phi_1, \dots, \phi_L)$. When applied to $|0\rangle$, this results in the state $\mathcal{S}|0\rangle$ and the transition probability $p(\theta) = |\langle 1|\mathcal{S}|0\rangle|^2$ in θ coordinates. As θ depends on position x_i , a map from spatial coordinates to transition probability is achieved through $s(x) = p(\theta(x))$.

The criteria of unambiguity and optimality can now be expressed as constraints on the form of $s(x)$. Unambiguity means that $s(x)$ has only a single sharp peak in some domain of x so that excitation with high probability only occurs if the system lies in some small contiguous region of space Δ , which defines, through its width $|\Delta|$, the resolution $r \approx |\Delta|$. Noting that $p(\theta)$ is periodic in $\theta \rightarrow \theta \pm 2\pi$

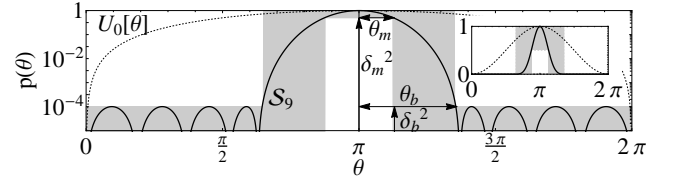


FIG. 2: Transition probability $p(\theta)$ of the sequence \mathcal{S}_L (solid) plotted for $L = 9$ in comparison to a single rotation $U_0[\theta]$ (dotted). The range of the envelope $p(\theta; \theta_b, \theta_m)$ is shaded. Primary features of \mathcal{S}_L are sidelobes of uniform bounded error δ_b^2 , and a central peak with width parameters θ_b, θ_m that scale as $\sim 1/L$. The inset plots the same on a linear scale.

and, for odd L , necessarily peaks at $p(\theta = \pi) = 1$, unambiguity is possible if no other large peaks occur in the domain of $0 \leq \theta(x) < 2\pi$ and $\theta(x)$ varies monotonically with x . For example, a Gaussian diffraction-limited beam with spatial profile $\Omega(x) = \Omega_0 e^{-x^2/4\lambda^2}$ restricted to $x > 0$ and the choice $\Omega_0 t = \sqrt{e}\pi$ suffices and will be used in what follows. With this choice, and assuming unambiguous $p(\theta)$, the only peak in $s(x)$ occurs at $x = \sqrt{2}\lambda$, exactly where $\theta = \pi$, and where also the gradient of $\Omega(x)$ is steepest so that the width of the peak is minimized. Expressed in θ coordinates, the peak width of $2\theta_b = |\Delta|\theta'$ is illustrated in Fig. 2, where $\theta' = \max_x \left| \frac{d\theta(x)}{dx} \right|$. In particular, optimality means that the width of this single peak scale like $\theta_b \sim \frac{1}{L}$ – any better scaling would permit a means to beat the Heisenberg limit.

Both unambiguity and optimality are satisfied by our new family of pulse sequences \mathcal{S}_L , which realize the transition profile

$$p_L(\theta; \delta_b) = \left| \frac{T_L[\beta_L(\delta_b) \sin(\frac{\theta}{2})]}{T_L[\beta_L(\delta_b)]} \right|^2, \quad (1)$$

plotted in Fig. 2, where $T_L[x] = \cos[L \cos^{-1}(x)]$ is the L^{th} Chebyshev polynomial, and $\beta_L(\delta_b) = T_{L-1}[\delta_b^{-1}]$. Primary features of the function $p_L(\theta; \delta_b)$ include an optimally narrow, like $\sim \frac{1}{L}$, central peak given a uniform bound δ_b^2 on sidelobes [20]. We find it useful to consider the half-width θ_b of the central peak at sidelobe height δ_b^2 and θ_m at arbitrary heights $\delta_m^2 > \delta_b^2$ (Fig. 2) with ratio of widths $R = \theta_b/\theta_m > 1$:

$$\theta_b(L) = \frac{2}{L} \text{arcsech}(\delta_b) + \mathcal{O}\left(\frac{1}{L^3}\right), \quad (2)$$

$$R = 1 / \sqrt{1 - \left(\frac{\text{arcsech}(\delta_b/\delta_m)}{\text{arcsech}(\delta_b)} \right)^2} + \mathcal{O}\left(\frac{1}{L^2}\right),$$

The phases (ϕ_1, \dots, ϕ_L) that implement \mathcal{S}_L for arbitrarily large L are elegantly described in closed-form. We first consider the broadband variant $\mathcal{S}_L^B = (\chi_1, \dots, \chi_L)$ which realizes $p_L^B(\theta; \delta_b) = 1 - p_L(\theta - \pi; \delta_b)$ and is related to \mathcal{S}_L via the toggling transformation $\phi_k = (-1)^k \chi_k + 2 \sum_{h=1}^{k-1} (-1)^h \chi_h$ [21]. That the three pulse member $\mathcal{S}_3^B =$

$(\chi, 0, \chi)$ has $\chi = 2 \tan^{-1} \left[\tan(\pi/3) \sqrt{1 - \beta_3^{-2}(\delta_b)} \right]$ is easily verified. As the phases of \mathcal{S}_3^B form a palindrome [18, 19], \mathcal{S}_3^B implements an effective rotation of angle θ_e , defined through $1 - p_L^B(\theta; \delta_b) = \cos^2(\theta_e/2)$, about some axis in the \hat{x} - \hat{y} plane. Thus replacing each base pulse in $\mathcal{S}_{L_2=3}^B[\delta_b]$ with a different sequence $\mathcal{S}_{L_1=3}^B[1/\beta_{L_2}(\delta_b)]$ produces the transition profile $p_{L_1 L_2}^B(\theta; \delta_b)$ by repeatedly applying the semigroup property $T_n[T_m[x]] = T_{nm}[x]$ of Chebyshev polynomials. For $L_2 = 3$ and any odd L_1 , this corresponds exactly to the transition profile of $\mathcal{S}_{3L_1}^B[\delta_b] = (\psi, 0, \psi) \circ \mathcal{S}_{L_1}^B[1/\beta_3(\delta_b)]$, where \circ defines a nesting operator $(a_1, a_2, \dots) \circ (b_1, b_2, \dots) = (a_1 + b_1, a_1 + b_2, \dots, a_2 + b_1, a_2 + b_2, \dots)$. As we provide $L_1 = 3$, by induction the phases required for $\mathcal{S}_{3^n}^B[\delta_b]$ and $\mathcal{S}_{3^n}[\delta_b]$ can be obtained in closed form as a function of δ_b for all $n \in \mathbb{Z}^+$.

After \mathcal{S}_L is applied for some choice of beam position x_c , a measurement of $|\psi\rangle$ extracts encoded positional information. As visualized with the envelope in Fig. 2:

$$p(\theta; \theta_b, \theta_m) = \begin{cases} \geq \delta_m^2, & |\theta - \pi| \leq \theta_m, \\ \in [0, 1], & \theta_m < |\theta - \pi| < \theta_b, \\ \leq \delta_b^2, & \text{otherwise,} \end{cases} \quad (3)$$

if $|1\rangle$ is obtained after a measurement, the object is located with high probability in the central peak, corresponding to the spatial interval Δ^b of width $|\Delta^b| = 2\theta_b/\theta'$ centered on x_c . Conversely, if $|0\rangle$ is obtained, then the object is located outside, in $I \setminus \Delta^m$, with high probability, where Δ^m is also centered on x_c with width $|\Delta^m| = 2\theta_m/\theta'$. However, projection noise means that false positives or negatives can still occur. Fortunately, these can be made exponentially improbable by initializing to $|0\rangle$, and taking l repeats.

The probability P of an incorrect classification, that is, assigning an estimate x_e to an interval that does not contain x_i is an elementary exercise in probabilities. We summarize: Over l repetitions, we measure the outcome $|1\rangle$ k times. If $k/l \geq \bar{p} = (\delta_m^2 + \delta_b^2)/2$, we assign $x_e \in \Delta^b$. Else, we assign $x_e \in I \setminus \Delta^m$. Thus

$$\begin{aligned} P &= \max(P_1, P_2) \leq \exp[-l(\delta_m^2 - \delta_b^2)^2/2], \\ P_1 &= \Pr[x_e \in I \setminus \Delta^m | x_i \in \Delta^m] = \Pr[k/l < \bar{p} | x_i \in \Delta^m], \\ P_2 &= \Pr[x_e \in \Delta^b | x_i \in I \setminus \Delta^b] = \Pr[k/l \geq \bar{p} | x_i \in I \setminus \Delta^b], \end{aligned} \quad (4)$$

where P is bounded by Hoeffding's inequality applied to binomial distributions [22]. Thus x_e can be reliably classified to either inside or outside a region of width $|\Delta| \sim \frac{1}{L}$ in a constant number of ~ 1 measurements.

A key insight allows us to sidestep the $\sigma \sim \frac{1}{\sqrt{t}}$ scaling of projection noise arising from accumulating statistics indefinitely. Once the object has been classified to some interval Δ^b with high probability, a sequence that is K times longer than \mathcal{S}_L can be applied to query subintervals of width K times smaller than Δ^b . As the width of these subintervals scale optimally like $\sim \frac{1}{L}$ in Eq. 2, it is never profitable, in the coherent regime, to accumu-

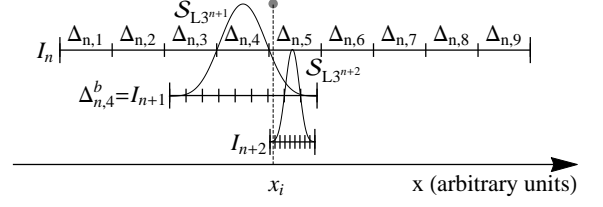


FIG. 3: Two iterations of the logarithmic search illustrated for an object located at x_i . At the n^{th} iteration, the object has been localized to the interval $x_i \in I_n$. I_n is split into D intervals Δ_d , and $\mathcal{S}_{L_{3^{n+1}}}$ with base width Δ_d^b is applied to each interval l times. The first positive classification to Δ_d^b for any d further narrows the object position to $x_i \in \Delta_d^b = I_{n+1}$. In this example, $R|\Delta_d^b| \approx |I_n|$, $R \approx 3$, $\delta_m^2 = 1/2$, $\delta_b^2 = 10^{-4}$, $K = 3$.

late more than a constant number of statistics. Rather, L should be increased in geometric progression as far as coherence times allow. In other words, imaging proceeds by logarithmic search, illustrated in Fig. 3 for $x_i \in I_0$ initially known only to be in the region I_0 of width $|I_0| \lesssim \lambda$. Although this process is conceptually similar to binary search, we must account for two key differences: 1) queries are corrupted by projection noise and 2) the accept and reject intervals are asymmetric i.e. $\Delta^b \neq \Delta^m$.

The search is initialized by choosing the largest L_0 such that $|I_0| < 2\theta_b(L_0)/\theta'$ followed by $n = 1, \dots, M$ iterations of a recursive process. The n^{th} iteration involves three steps. First, I_{n-1} is split into D smaller subintervals of equal width, each centered on $x_{n,d}$. Here, $D = \lceil KR \rceil$, $K \in \mathbb{Z}^+$, and $d = 1, \dots, D$. Second, the classification procedure involving l applications of \mathcal{S}_{L_n} , where $L_n = L_0 K^n$, is then applied for each d with $x_c = x_{n,d}$ until for some d , x_e is classified into $x_e \in \Delta_{n,d}^b$. Third, we update $I_n = \Delta_{n,d}^b$, which is of width $|I_n| = \frac{|I_{n-1}|}{K}$. By induction over M iterations, x_e lies in an interval width $|I_M| \approx |I_0| \left(\frac{1}{K}\right)^M$. Since $K > 1$, exponential precision $|I_M|$ is achieved in only a linear number of $\mathcal{O}(M)$ state initializations and measurements! Any misclassification of $x_e \in \Delta_{n,d}^b$ such that $x_i \notin \Delta_{n,d}^b$ will be detected in the next iteration as the probability of misclassifying $x_e \in \Delta_{n+1,d}^b$ again becomes vanishingly small like $\mathcal{O}(P^2)$, as seen from Eq. 4. In that case, the previous iteration is repeated. Assuming $x_i \in I_M$ is uniformly distributed, the standard deviation is $\sigma \approx \frac{|I_0|}{K^M \sqrt{12}} (1 + \mathcal{O}(P))$.

The runtime t of this logarithmic search is a geometric sum over iterations $n = 1, \dots, M$, each involving an expected number $E = Dl/2 + \mathcal{O}(P)$ applications of \mathcal{S}_{L_n} . Letting, $\Omega' = \theta'/\tau$, we have

$$\begin{aligned} t &= E \sum_{n=1}^M \tau L_n \approx \frac{E|I_0|\theta' L_0 K}{K-1} \frac{K^M - 1}{K^M} \frac{1}{|I_M|\Omega'} \\ &\approx \frac{4EK \text{arcsech}(\delta_b)}{K-1} \frac{1}{|I_M|\Omega'} \approx \frac{2EK \text{arcsech}(\delta_b)}{\sqrt{3}(K-1)} \frac{1}{\sigma\Omega'}, \end{aligned} \quad (5)$$

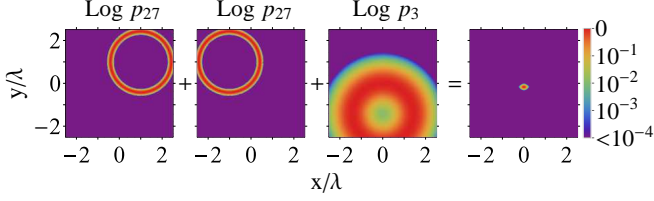


FIG. 4: (Color online) Demonstration of using three Gaussian beams in two dimensions, $\theta(x, y) = \sqrt{e\pi}e^{-(x^2+y^2)/4\lambda^2}$, and exploiting the strongly peaked log transition probability $\log p_L \equiv \log p_L(\theta(x, y); 10^{-2})$ to locate the object at $(x_i, y_i) = (0, 0)$. The beam centers are placed at $(1, 1)$, $(-1, 1)$, $(0, -\sqrt{2})$ and sequences $\mathcal{S}_{27}, \mathcal{S}_{27}, \mathcal{S}_3$ implemented, respectively.

where the approximations $K^M - 1 \approx K^M$, $|I_0| \approx 2\theta_b(L_0)/\theta'$, $\sigma \approx |I_M|/\sqrt{12}$ are made.

Thus, in Eq. (5) we have arrived at our final result: an estimate of object position x_e with standard deviation $\sigma = \frac{1}{\Omega'} \mathcal{O}(\frac{1}{t})$ exhibiting a Heisenberg-limited scaling with time, and requiring $M = \mathcal{O}(\log \frac{1}{\sigma})$ measurements. The most straightforward minimization of the constant factors requires the choices of 1) shortest wavelength λ and 2) strongest drive Ω_0 . However, these parameters are often fixed by experimental constraints. One could then optimize over the independent variables δ_b, δ_m, l, K . For example, inserting $K = 3, l = 5, \delta_b^2 = \frac{7}{20}, \delta_m^2 = \frac{13}{20}$ into Eq. 5, evaluating E to $\mathcal{O}(P^2)$, and Eq. 4 exactly gives $t \approx \frac{26}{\Omega'\sigma}$.

Notably, our imaging procedure only gracefully degrades in the presence noise found in real systems with any finite coherence time τ_c . Noise replaces \mathcal{S} with an implementation-dependent quantum channel $\mathcal{E}(\rho)$ acting on the initial state $\rho_i = |0\rangle\langle 0|$ to produce the output $\rho_{noise} = \mathcal{E}(\rho_i)$, in comparison to the ideal case of $\rho_{ideal} = \mathcal{S}\rho_i\mathcal{S}^\dagger$. As the trace distance [8] $\text{TrD}(\rho_{ideal}, \rho_{noise}) = \gamma$ bounds the difference in measurement probabilities using any measurement basis, noise shifts the envelope in Eq. 3 by $\delta_b^2 \rightarrow \delta_b^2 + \gamma, \delta_m^2 \rightarrow \delta_m^2 - \gamma$ and modifies the misclassification probability in Eq. 4 to

$$P \leq \exp[-l(\delta_m^2 - \delta_b^2 - 2\gamma)^2/2] \ll 1, \quad (6)$$

As long as $\gamma < \frac{1}{2}$, classification succeeds *independent* of the noise model as we can always satisfy Eq. 6 by some choice of δ_b, δ_m , and $l(\gamma) \propto (\delta_m^2 - \delta_b^2 - 2\gamma)^{-2}$. Success for $\gamma \geq \frac{1}{2}$ depends on details of the noise model. Of course, γ generally increases with sequence length, such as in a completely depolarizing channel where $\gamma_n = \frac{1}{2}(1 - e^{-tL_n/\tau_c})$. For fixed δ_m, δ_b , the runtime in Eq. 5 becomes $t \propto \sum_{n=1}^M l(\gamma_n)K^n$. As the final precision $\sigma \propto \frac{1}{K^M}$, the instantaneous scaling in the presence of noise

$$\begin{aligned} \frac{dt}{d(\sigma^{-1})} &= \frac{dt}{dM} \frac{dM}{d(\sigma^{-1})} \propto \frac{1}{(\delta_m^2 - \delta_b^2 - 2\gamma_M)^2} \\ &\propto 1 + \frac{2}{\delta_m^2 - \delta_b^2} \frac{\tau L_M}{\tau_c} + \mathcal{O}((\tau L_M/\tau_c)^2) \end{aligned} \quad (7)$$

shows clearly a continuous degradation from the noiseless Heisenberg-limited scaling $\lim_{\tau_c \rightarrow \infty} \frac{dt}{d(\sigma^{-1})} \propto 1$ to the statistical scaling $\frac{dt}{d(\sigma^{-1})} \propto \sqrt{t}$. In the regime of strong decoherence at $\tau L_M \sim \tau_c$ where higher orders dominate, accumulating statistics with \mathcal{S}_{L_M} and applying the law of large numbers becomes more time-efficient than using logarithmic search and correcting many misclassifications.

Generalizing our imaging scheme to higher dimensions is straightforward. Finding the (x_i, y_i, z_i) coordinates of an object in three dimensions is reducible to three separate one-dimensional problems by using three cylindrical Gaussian beams oriented about orthogonal axes with spatial profiles $\theta(x, y, z) = \sqrt{e\pi}e^{-s^2/4\lambda^2}$, $s \in \{x, y, z\}$. Illustrated in Fig. 4 is how one can also use three Gaussian beams with radial symmetry $\theta(x, y) = \sqrt{e\pi}e^{-(x^2+y^2)/4\lambda^2}$ to query the object position in two dimensions.

Extending the procedure to multiple $Q > 1$ objects also presents no fundamental difficulty. If there are Q objects, during iteration n , the classification procedure should be applied to *all* subintervals $\Delta_{n,d}^m$. Then, all subintervals that return a positive classification, i.e. $x_e \in \Delta_{n,d}^b$ are subject to subdivision and classification in the $(n+1)^{\text{th}}$ iteration. In particular, crosstalk can be suppressed by decreasing δ_b^2 by factor $\sim Q$. Therefore, in time $t \sim \frac{Q}{\sigma}$, all subintervals that contain objects will be found.

Many avenues of further inquiry are facilitated by the optimally narrow pulse sequences applied here for imaging. For example, the functional form of these pulse sequences match Dolph-Chebyshev window functions [20, 23] which have been studied in the context digital signal filtering [24, 25]. This hints at a deeper connection where the extensive machinery developed for signal processing could be applied to pulse sequences, interpreted as *quantum filters* [26]. Additionally, while the language of optical regimes of operation has been used here, the techniques presented are extremely generic and apply to the entire electromagnetic spectrum. With a fidelity of $\sim 10^{-6}$ per rotation in a pulse sequence, object positions can in principle be estimated with precision $\sim 10^{-6}\lambda$ in time scaling at the Heisenberg limit. At optical wavelengths, a practical limit may be imposed by the finite size of atoms, but exciting possibilities include using microwave wavelengths of $\sim 1\text{cm}$ to measure nanoscale $\sim 10\text{nm}$ features, or using radio waves in high-resolution magnetic resonance imaging, where instead of using magnetic field background gradients to provide nuclei or quantum dots spatially dependent resonance conditions, the spatial varying amplitude of the radio-frequency drive itself is used in conjunction with nuclear spins, which are known to have extremely long coherence times.

GHL acknowledges support from the ARO Quantum Algorithms program. TJY acknowledges support from the NSF iQuISE IGERT program. ILC acknowledges support from the NSF CUA.

-
- [1] E. Betzig and J. K. Trautman, *Science* **257**, 189 (1992).
 - [2] S. W. Hell, *Science* **316**, 1153 (2007).
 - [3] A. S. Trifonov, J. Jaskula, C. Teulon, D. R. Glenn, N. Bar-Gill, and R. L. Walsworth, *Advances in Atomic, Molecular, and Optical Physics* **62**, 279 (2013).
 - [4] M. Hofmann, C. Eggeling, S. Jakobs, and S. W. Hell, *Proceedings of the National Academy of Sciences of the United States of America* **102**, 17565 (2005).
 - [5] M. J. Rust, M. Bates, and X. Zhuang, *Nat Meth* **3**, 793 (2006).
 - [6] E. Betzig, G. H. Patterson, R. Sougrat, O. W. Lindwasser, S. Olenych, J. S. Bonifacino, M. W. Davidson, J. Lippincott-Schwartz, and H. F. Hess, *Science* **313**, 1642 (2006).
 - [7] E. Demkowicz-Dobrzanski, J. Kolodynski, and M. Guta, *Nat. Commun* **3**, 1063 (2012).
 - [8] M. A. Nielsen and I. L. Chuang, *Quantum Computation and Quantum Information* (Cambridge University Press, 2004).
 - [9] D. W. Berry, B. L. Higgins, S. D. Bartlett, M. W. Mitchell, G. J. Pryde, and H. M. Wiseman, *Phys. Rev. A* **80**, 052114 (2009).
 - [10] B. L. Higgins, D. Berry, S. Bartlett, M. Mitchell, H. M. Wiseman, and G. Pryde, *New Journal of Physics* **11**, 073023 (2009).
 - [11] W. M. Itano, J. C. Bergquist, J. J. Bollinger, J. M. Gilligan, D. J. Heinzen, F. L. Moore, M. G. Raizen, and D. J. Wineland, *Phys. Rev. A* **47**, 3554 (1993).
 - [12] D. Wineland, C. Monroe, W. M. Itano, D. Leibfried, B. E. King, and D. M. Meekhof, *J. Res. Natl. Inst. Stand. Technol.* **103**, 259 (1998).
 - [13] N. V. Vitanov, *Phys. Rev. A* **84**, 065404 (2011).
 - [14] C. M. Shappert, J. T. Merrill, K. R. Brown, J. M. Amini, C. Volin, S. C. Doret, H. Hayden, C. S. Pai, K. R. Brown, and A. W. Harter, *New Journal of Physics* **15**, 083053 (2013).
 - [15] C. Shen, Z. Gong, and L. Duan, *Phys. Rev. A* **88**, 052325 (2013).
 - [16] D. Le Sage, K. Arai, D. R. Glenn, S. J. DeVience, L. M. Pham, L. Rahn-Lee, M. D. Lukin, A. Yacoby, A. Komeili, and R. L. Walsworth, *Nature* **496**, 486 (2013).
 - [17] J. T. Merrill, S. C. Doret, G. D. Vittorini, J. P. Addison, and K. R. Brown, *arXiv:1401.1121v2 [quant-ph]* (2014).
 - [18] J. A. Jones, *Phys. Rev. A* **87**, 052317 (2013).
 - [19] G. Low, T. Yoder, and I. Chuang, *Phys. Rev. A* **89**, 022341 (2014).
 - [20] C. L. Dolph, *Proceedings of the Institute of Radio Engineers* **34**, 335 (1946).
 - [21] M. H. Levitt, *Progress in Nuclear Magnetic Resonance Spectroscopy* **18**, 61 (1986).
 - [22] W. Hoeffding, *Journal of the American Statistical Association* **58**, 13 (1963).
 - [23] F. Harris, *Proceedings of the IEEE* **66**, 51 (1978).
 - [24] A. Fettweis, *IEEE Transactions on Circuits and Systems* **31**, 31 (1984).
 - [25] A. Fettweis, *Proceedings of the IEEE* **74**, 270 (1986).
 - [26] A. Soare, H. Ball, D. Hayes, J. Sastrawan, M. J. J. Jarrott, M. C. and, X. Zhen, T. J. Green, and M. J. Biercuk, *arXiv: 1404*, 0820 (2014).